Photochemical and Photobiological Activity of Ru(II) Homoleptic and Heteroleptic Complexes Containing Methylated Bipyridyl-type Ligands

Lars Kohler,[a] Leona Nease,[b] Pascal Vo,[a] Jenna Garofolo,[b] David K. Heidary,[a] Randolph P. Thummel,[a]* and Edith C. Glazer[b]*

[a]Department of Chemistry, 112 Fleming Building, University of Houston, Houston, TX 77204-5003
[b]Department of Chemistry, University of Kentucky, Lexington, KY 40506

Supporting Information

Table of Contents

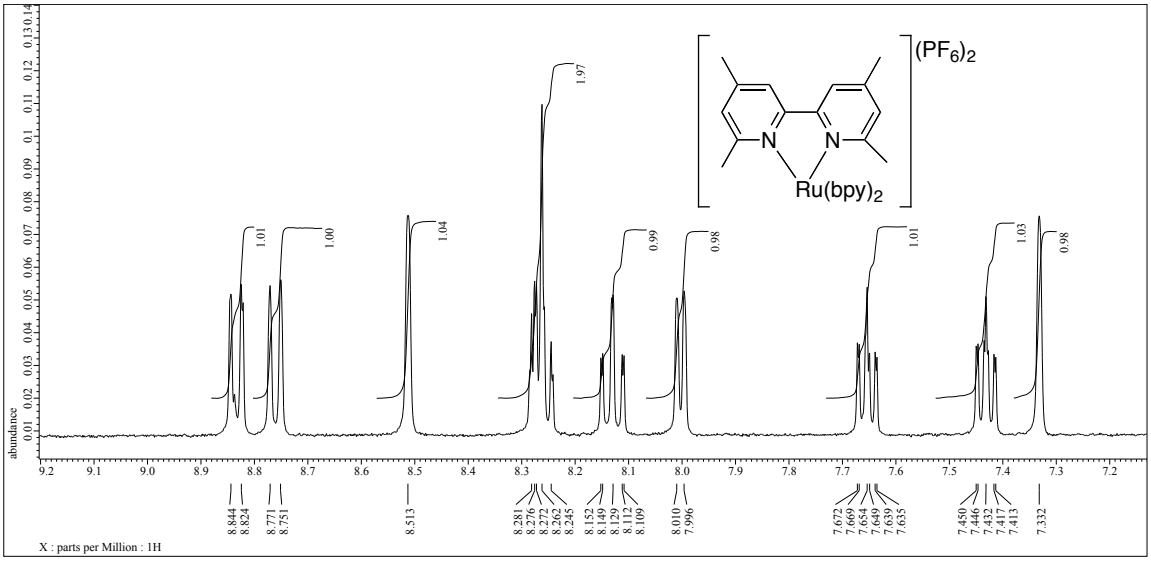

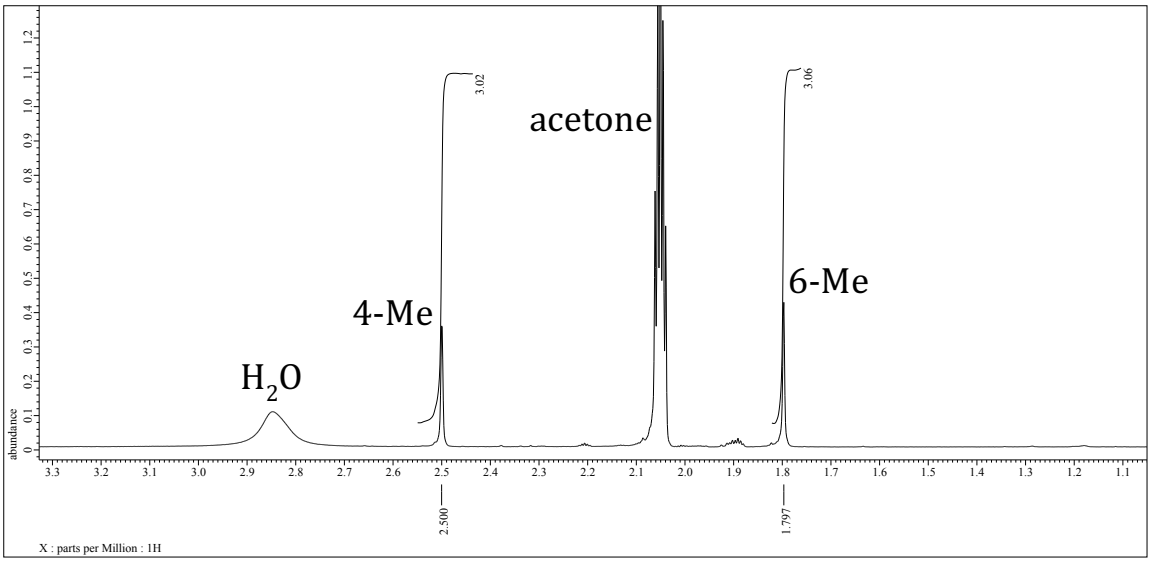

Figure S1. 500 MHz ^{1}H NMR spectrum of **1** in acetone-d_6 at 25 °C; top: downfield region; bottom: upfield region.

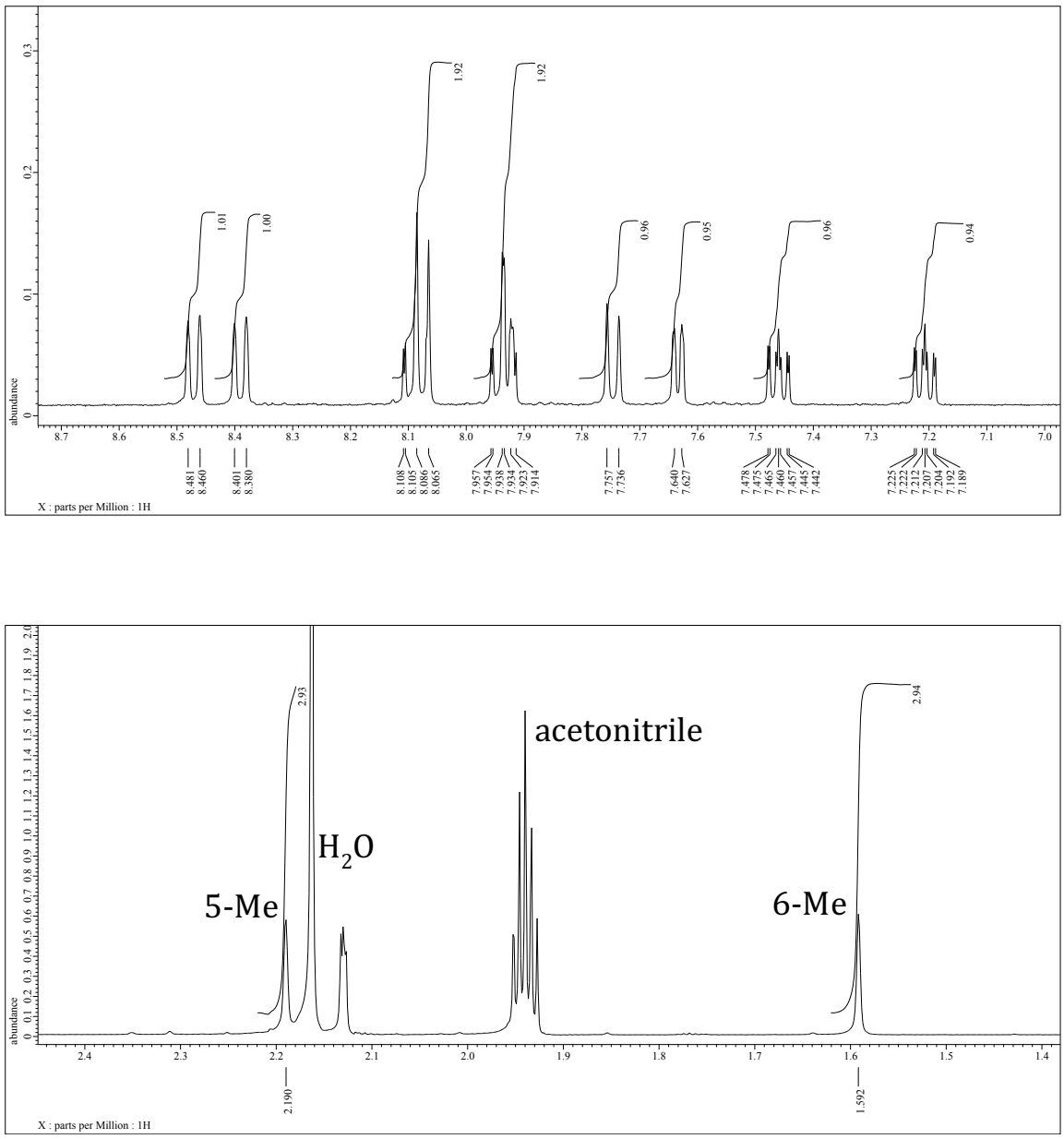

Figure S2. 500 MHz ^{1}H NMR spectrum of **2** in acetone-d_6 at 25 °C; top: downfield region; bottom: upfield region.

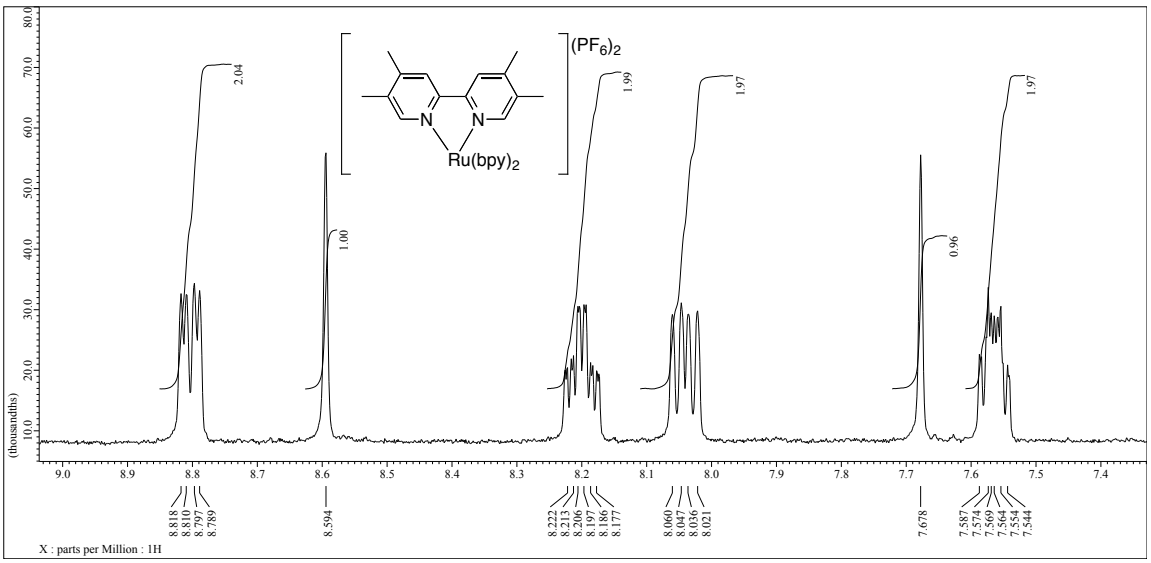

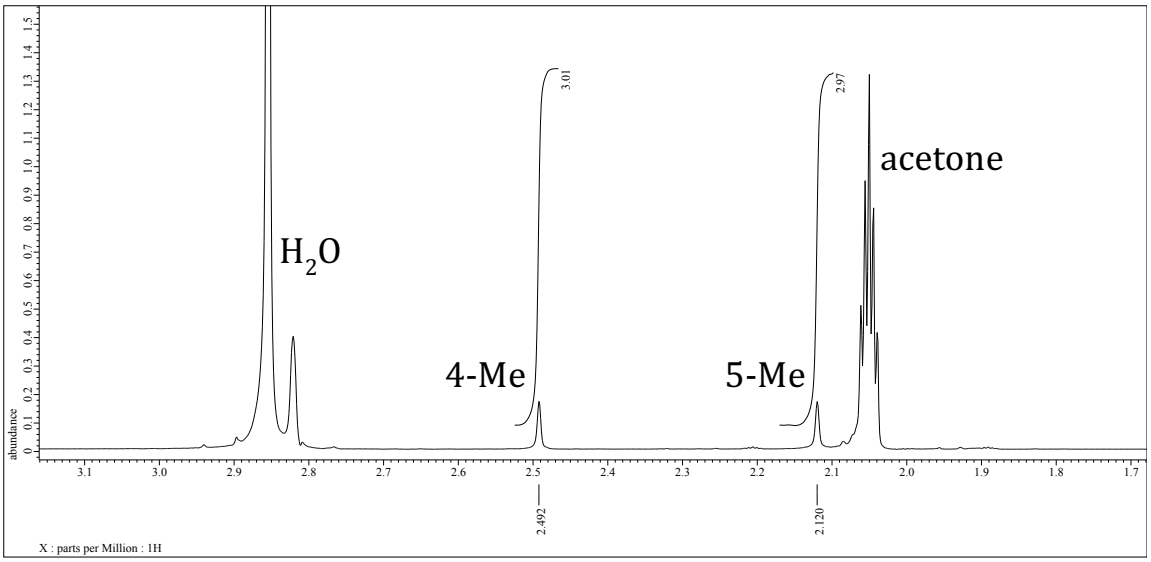

Figure S3. 500 MHz ^{1}H NMR spectrum of **3** in acetone-d_6 at 25 °C; top: downfield region; bottom: upfield region.

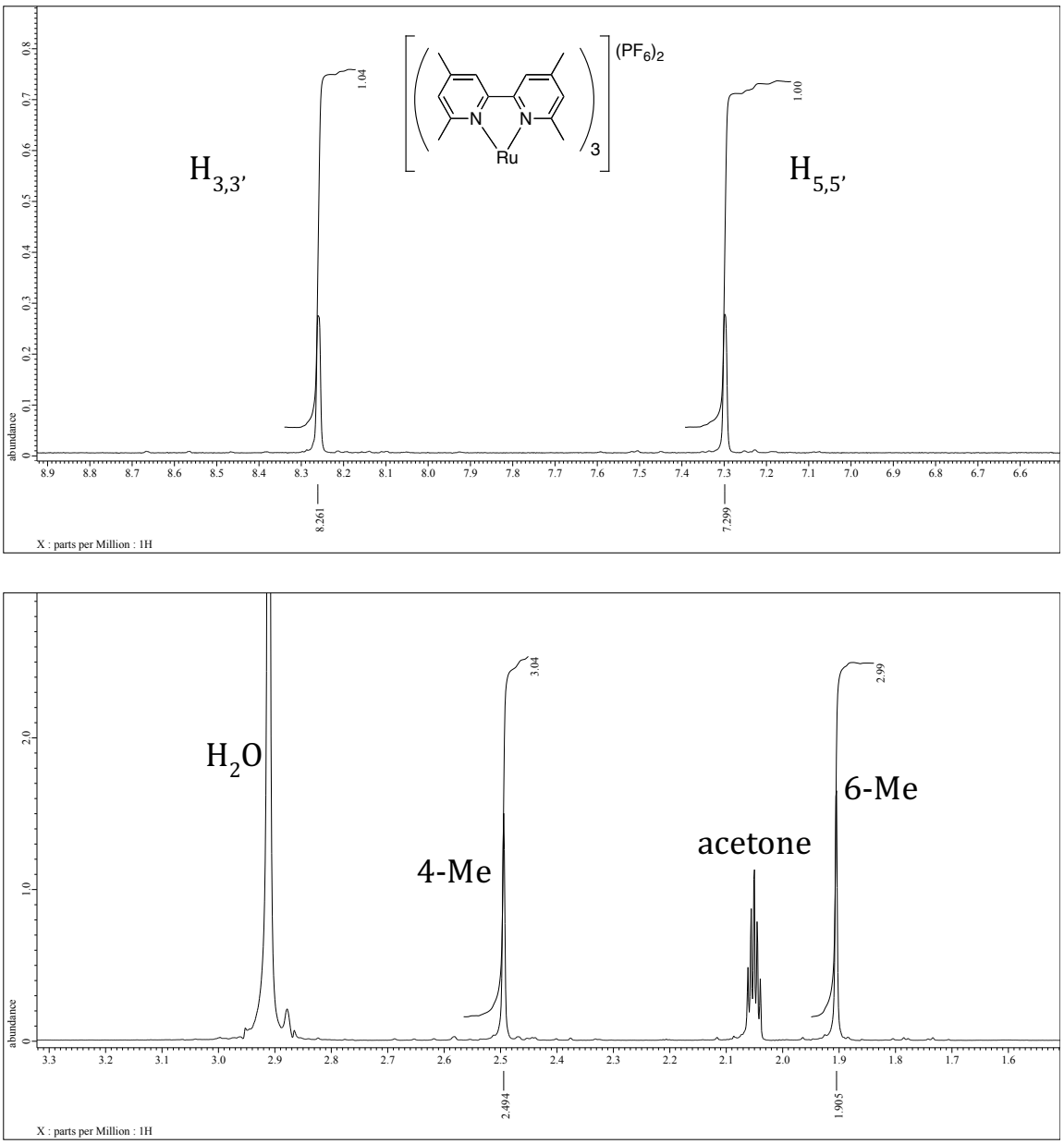

Figure S4. 500 MHz ^{1}H NMR spectrum of **4** in acetone-d_6 at 25 °C; top: downfield region; bottom: upfield region.

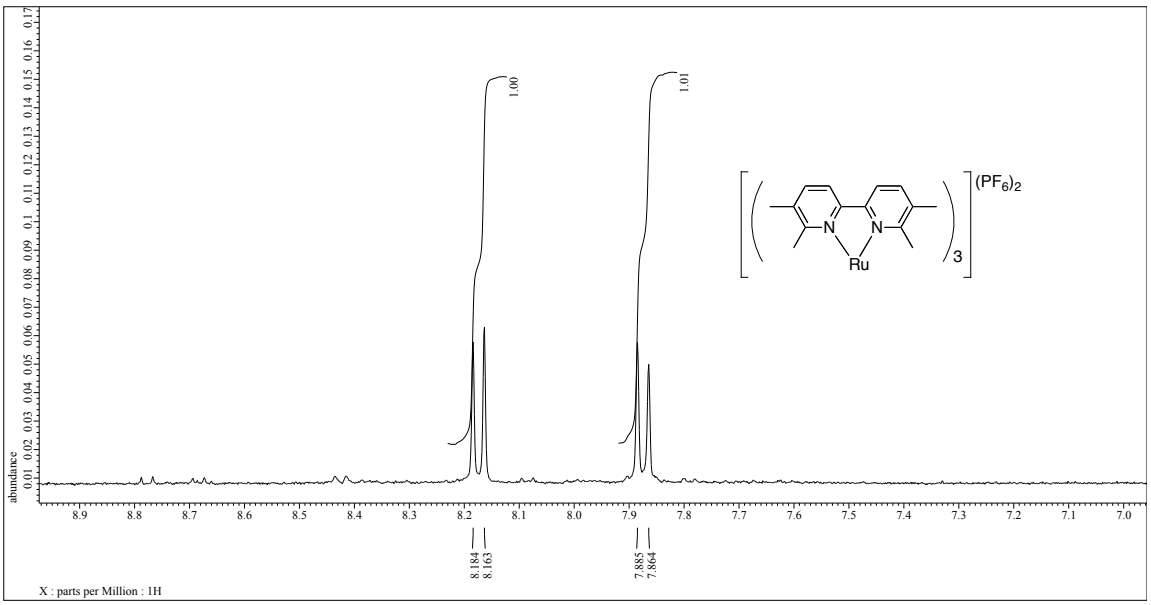

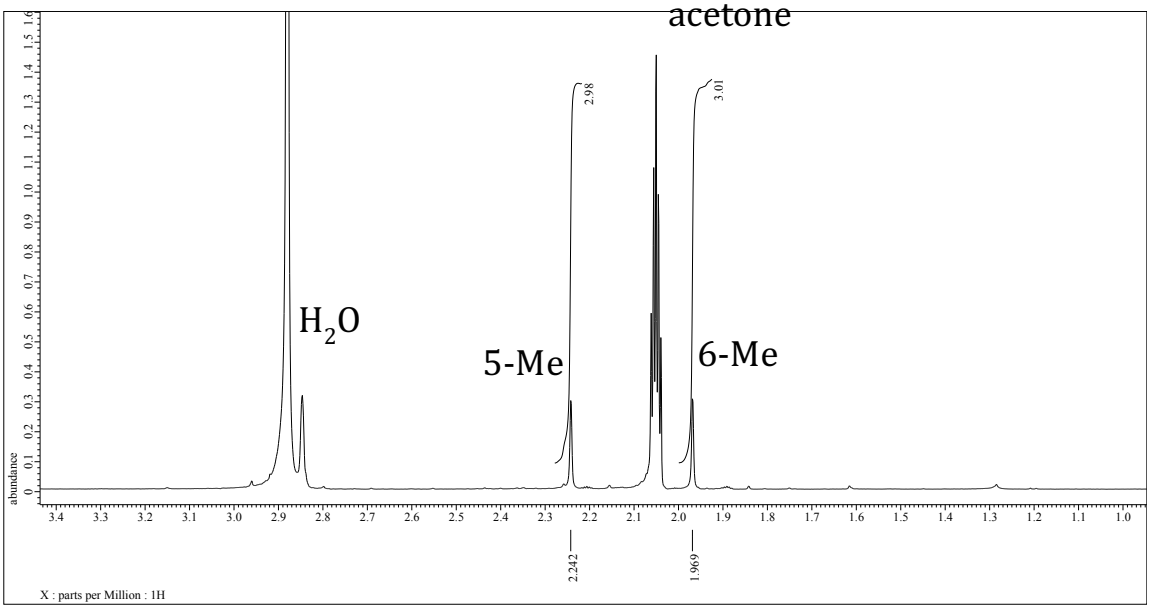

Figure S5. 500 MHz ^{1}H NMR spectrum of **5** in acetone-d_6 at 25 °C; top: downfield region; bottom: upfield region.

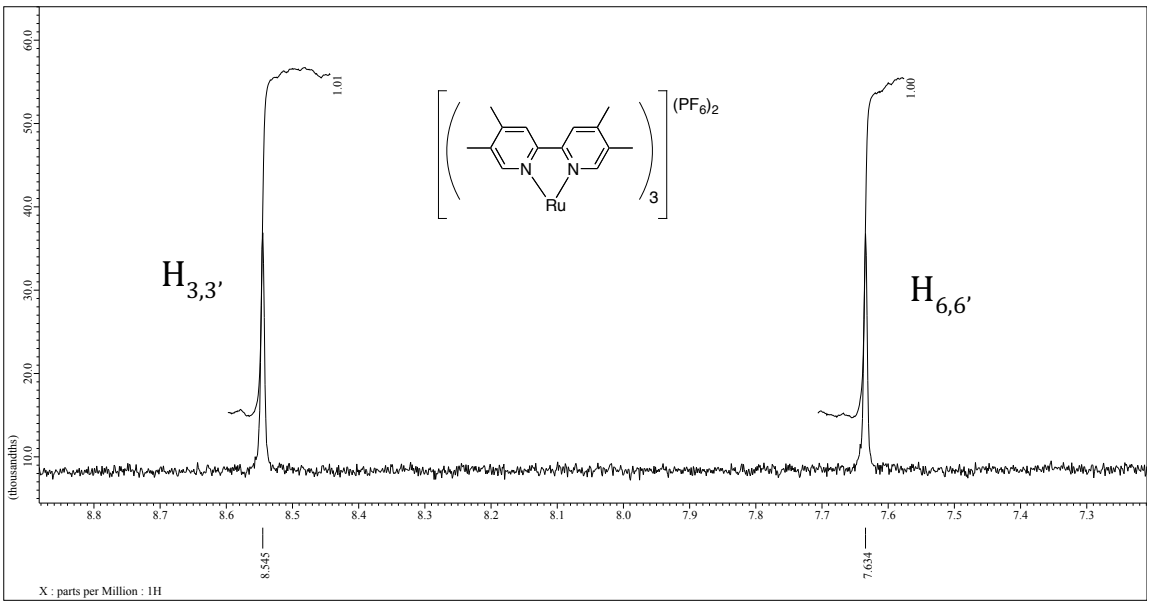

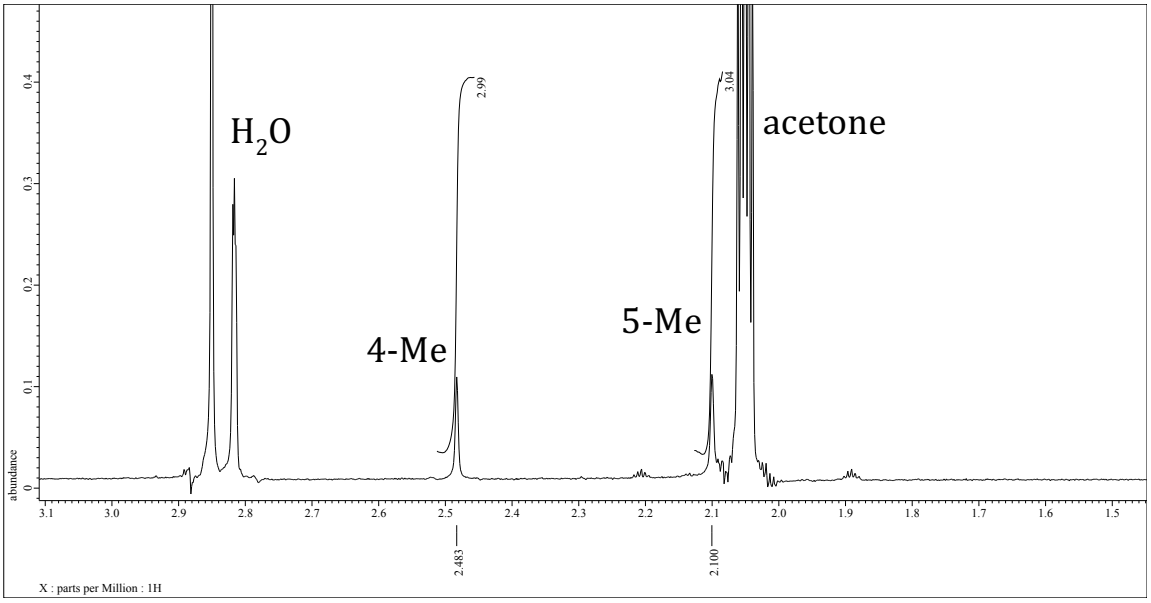

Figure S6. 500 MHz ^{1}H NMR spectrum of **6** in acetone-d_6 at 25 °C; top: downfield region; bottom: upfield region.

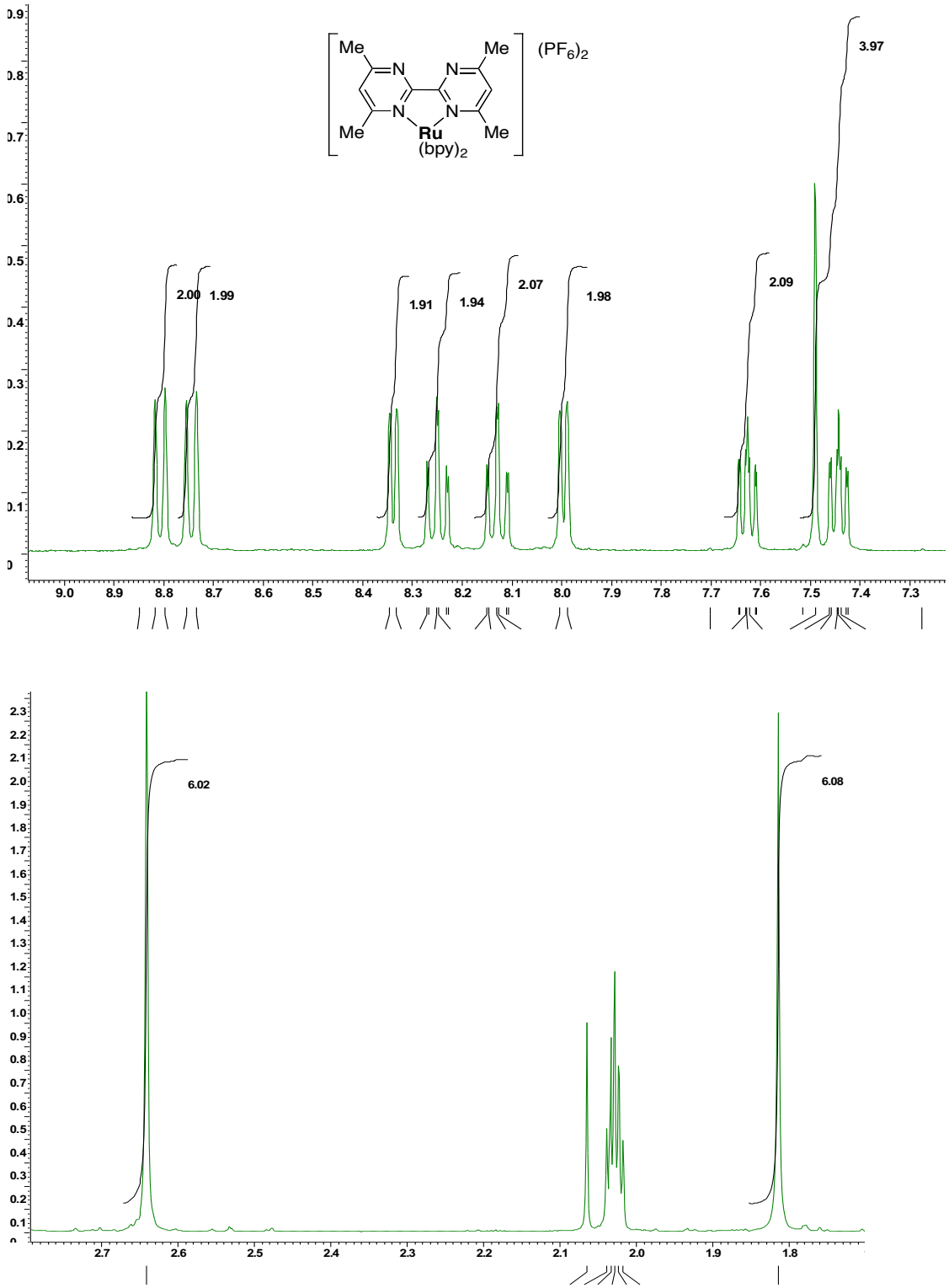

Figure S7. 500 MHz ^{1}H NMR spectrum of **7** in acetone-d_6 at 25 °C; top: downfield region; bottom: upfield region.

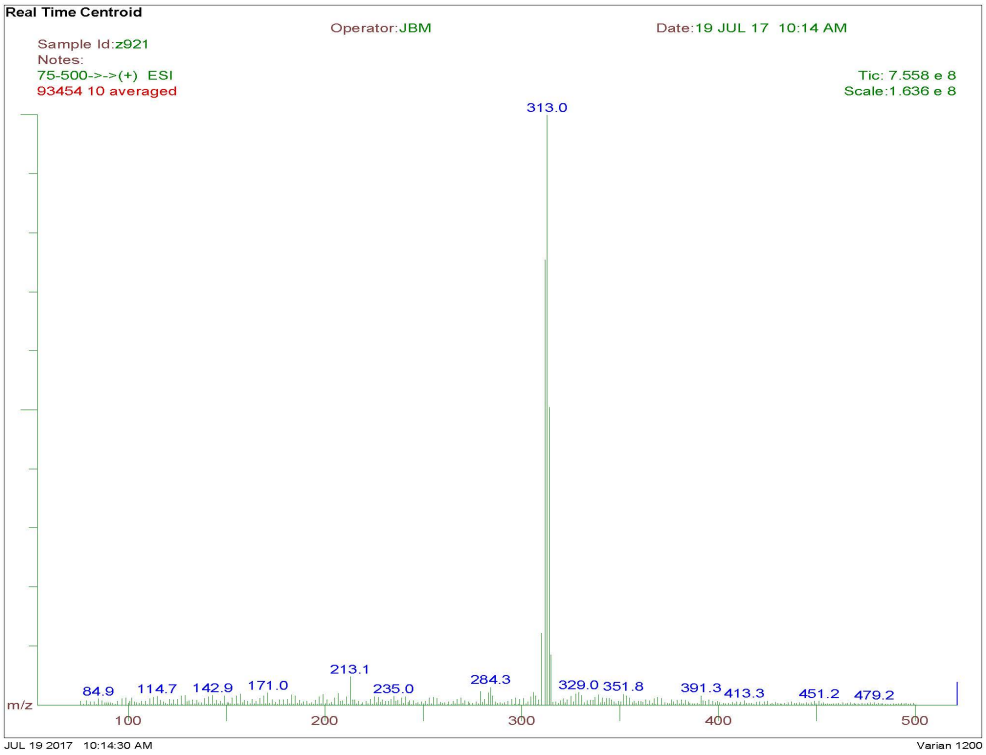

Figure S8. Mass spectrum of **1**.

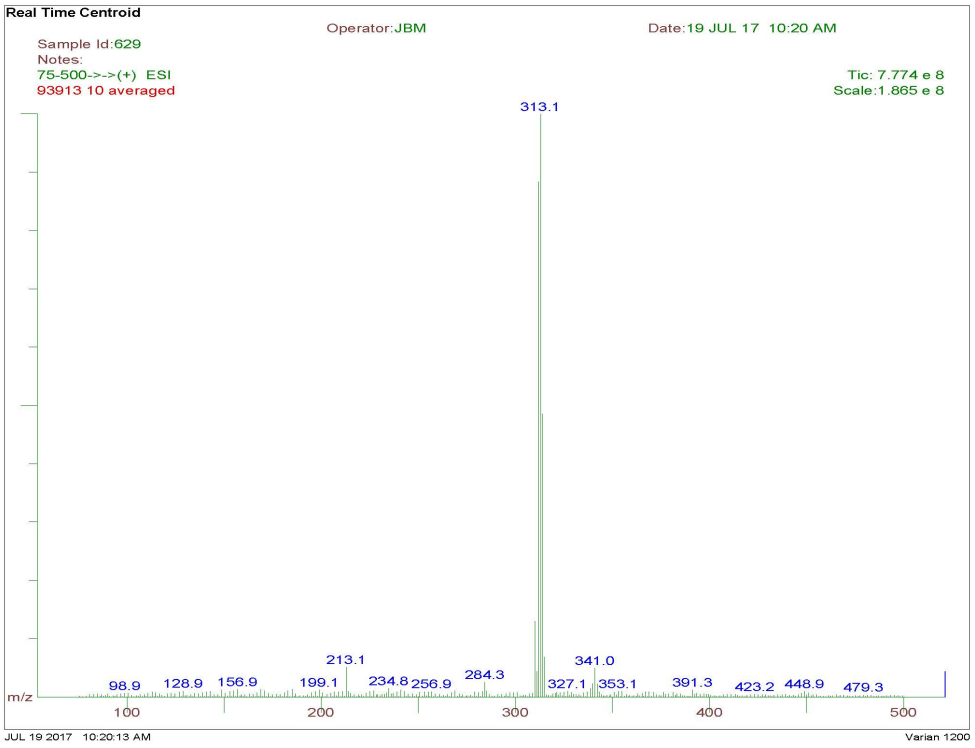

Figure S9. Mass spectrum of **2**.

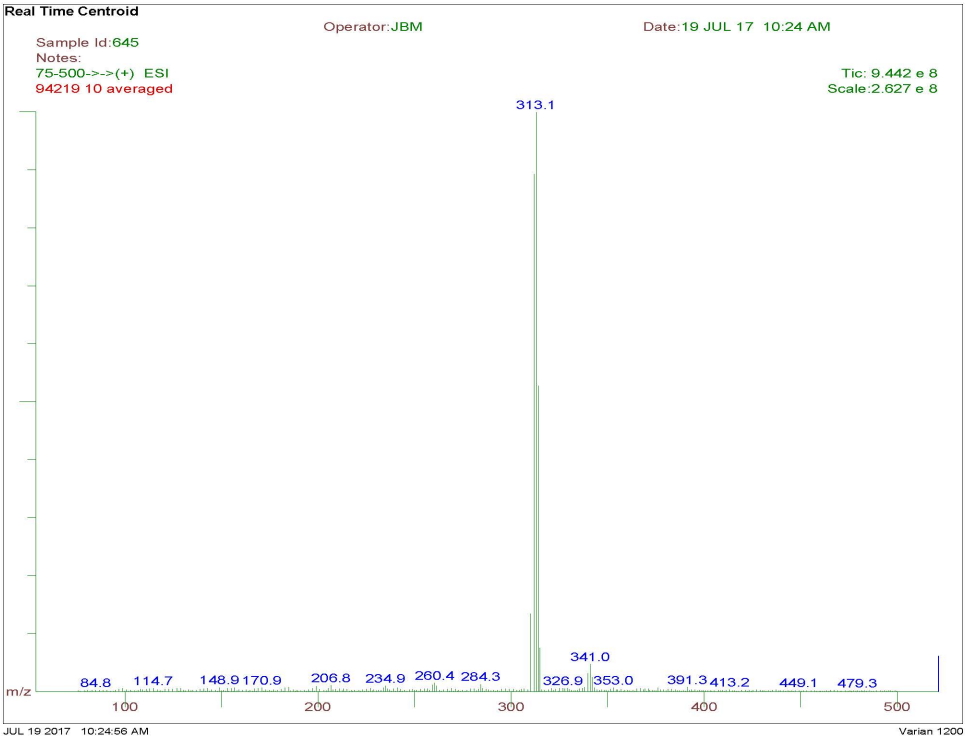

Figure S10. Mass spectrum of **3**.

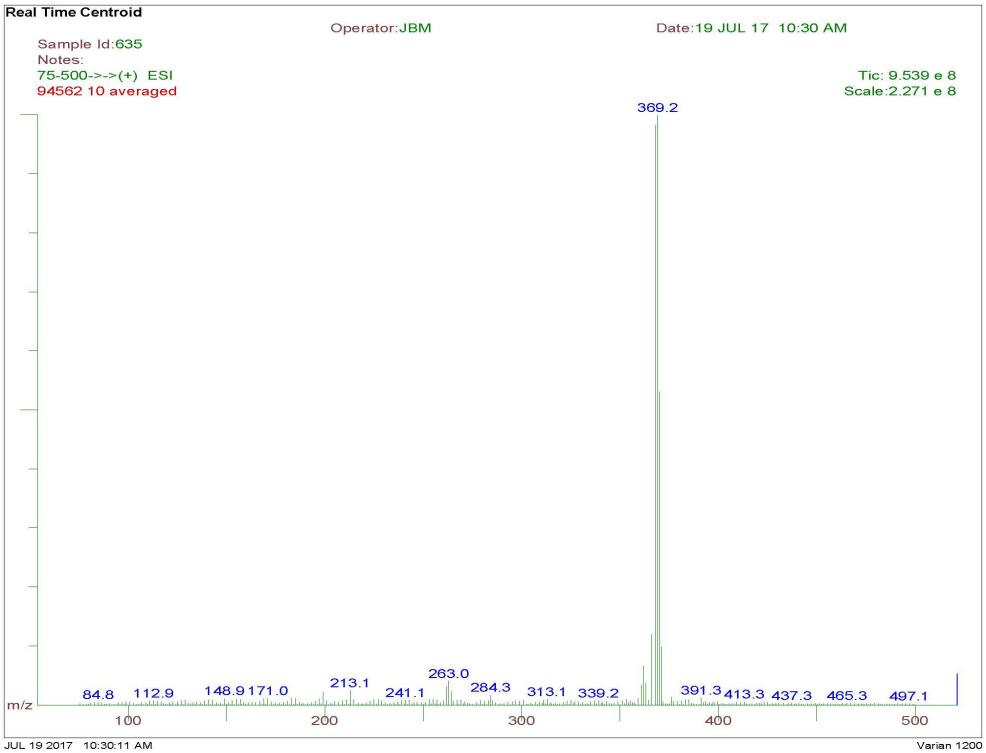

Figure S11. Mass spectrum of **4**.

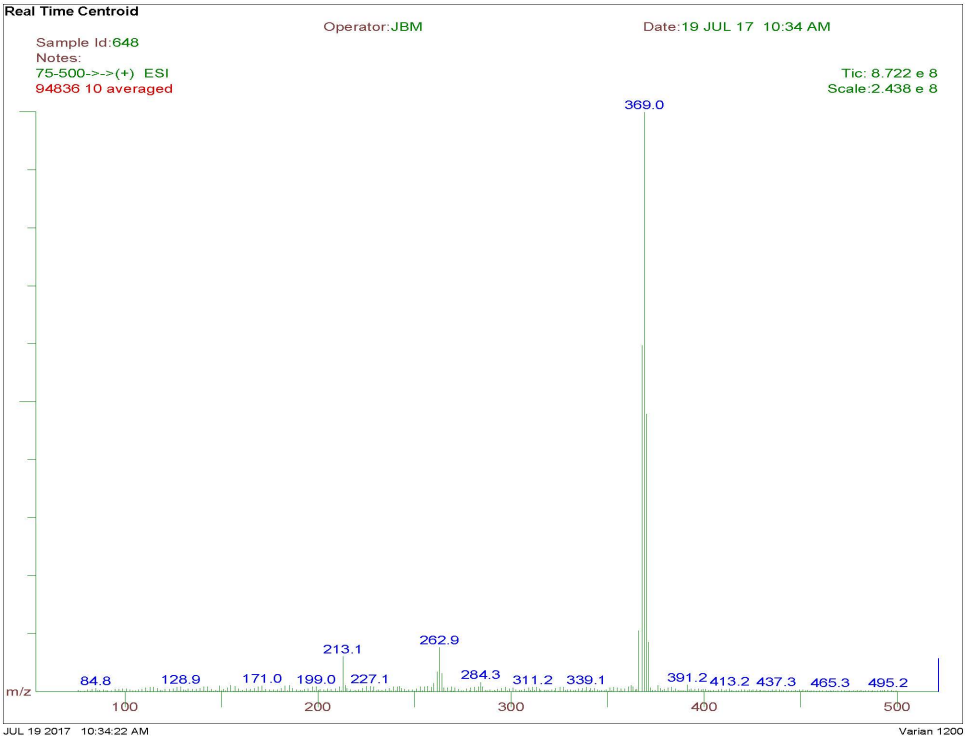

Figure S12. Mass spectrum of **5**.

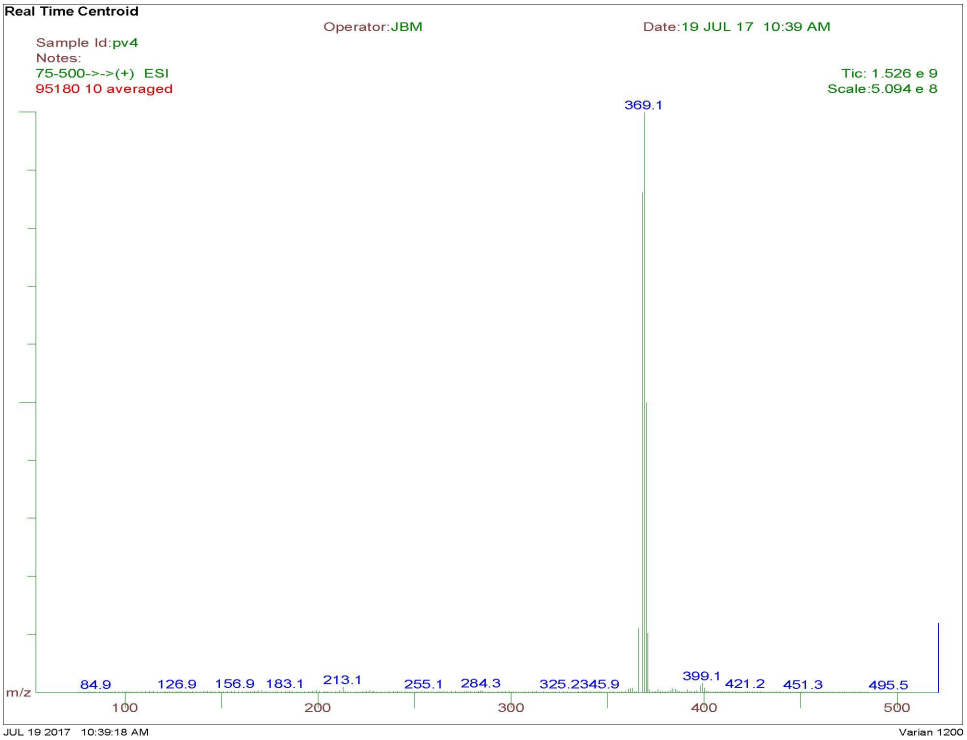

Figure S13. Mass spectrum of **6**.

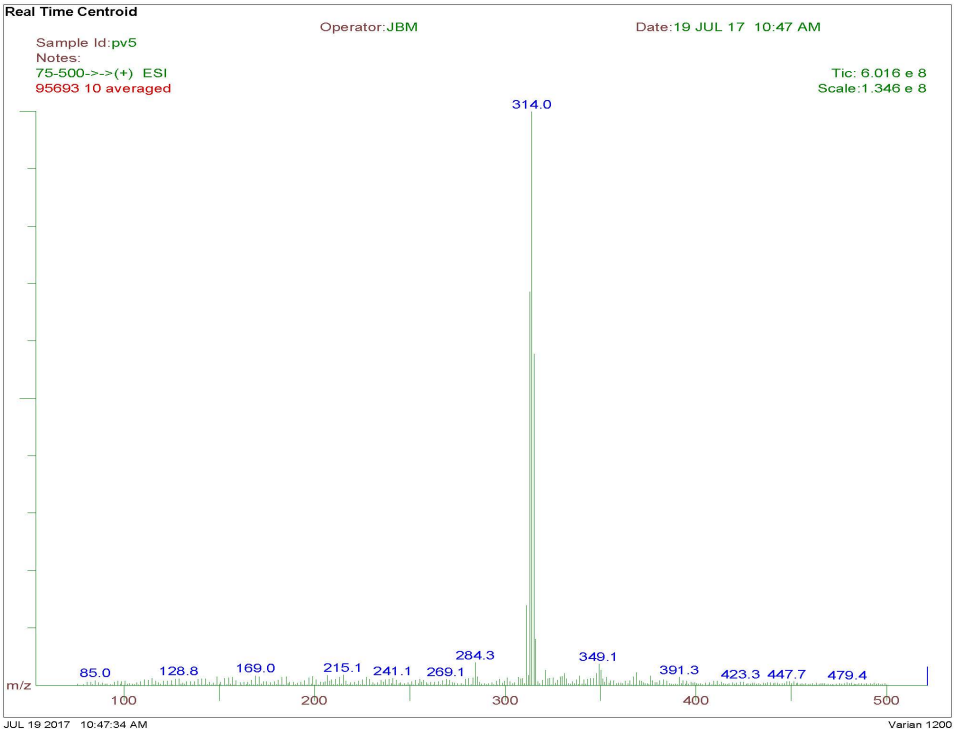

Figure S14. Mass spectrum of **7**.

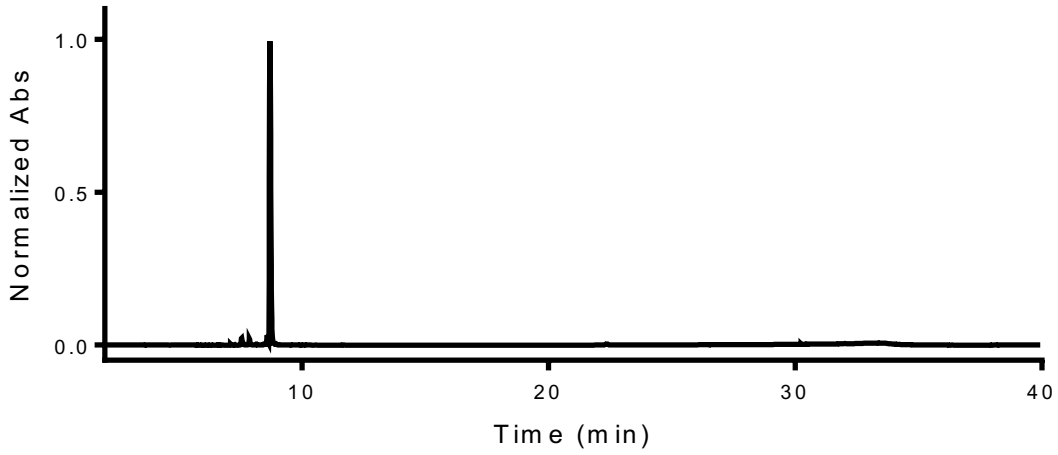

Figure S15. Analytical HPLC chromatogram of **1**.

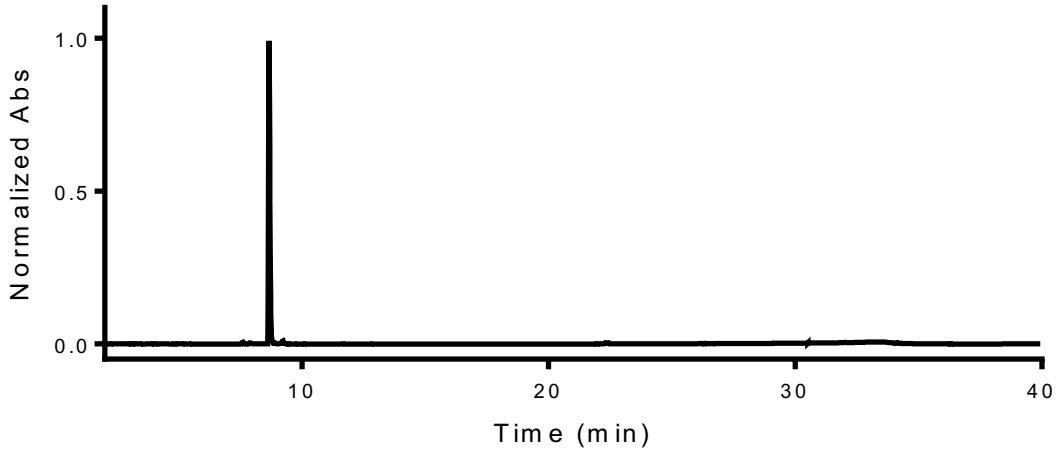

Figure S16. Analytical HPLC chromatogram of **2**.

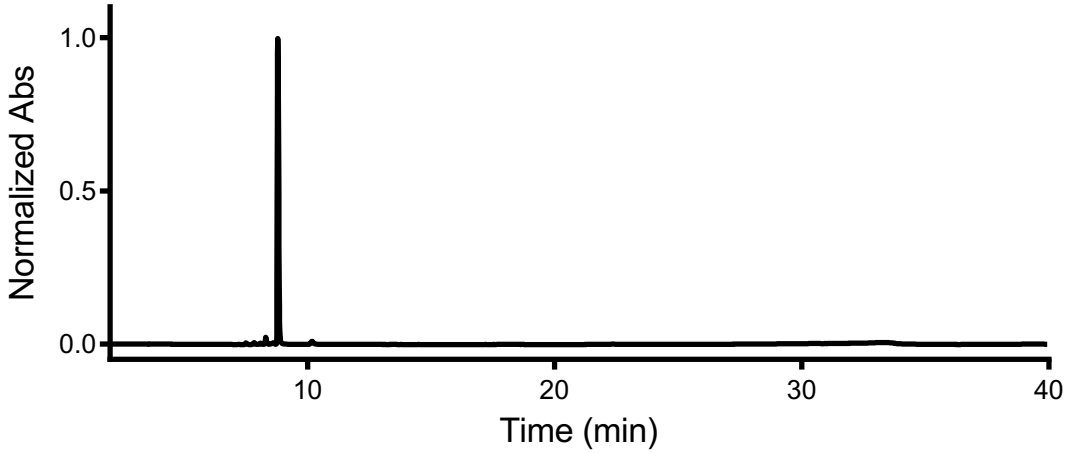

Figure S17. Analytical HPLC chromatogram of **3**.

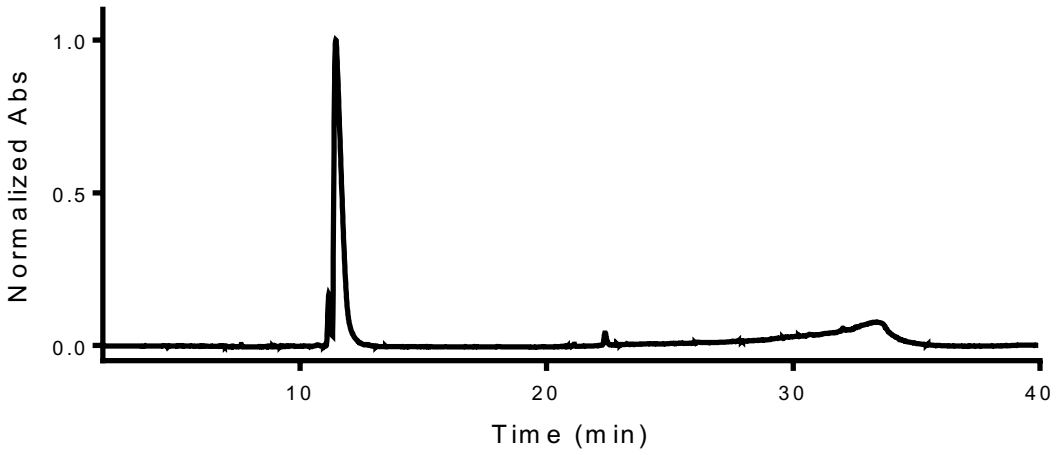

Figure S18. Analytical HPLC chromatogram of **4**.

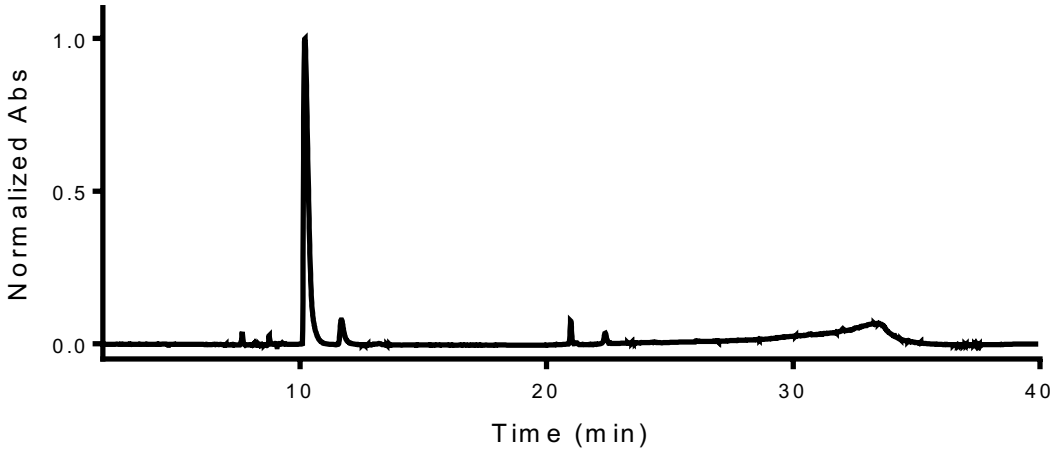

Figure S19. Analytical HPLC chromatogram of **5**.

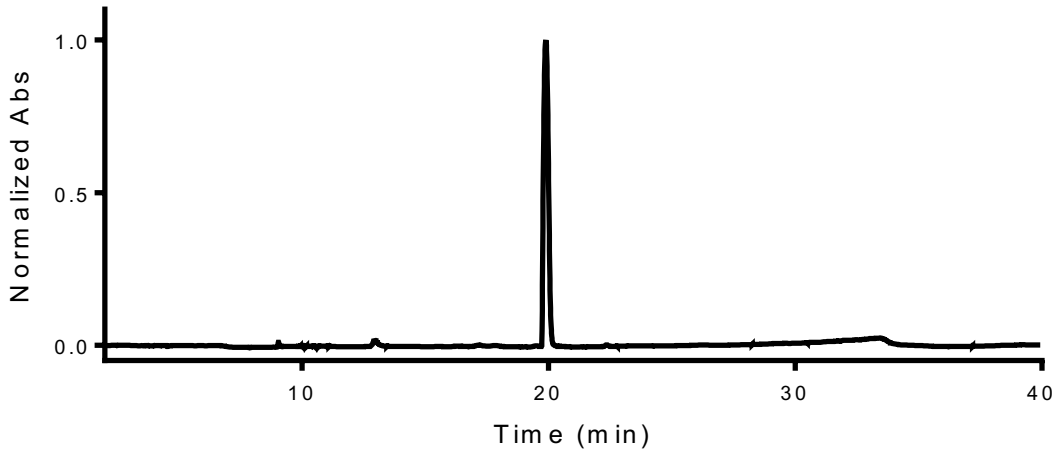

Figure S20. Analytical HPLC chromatogram of **6**.

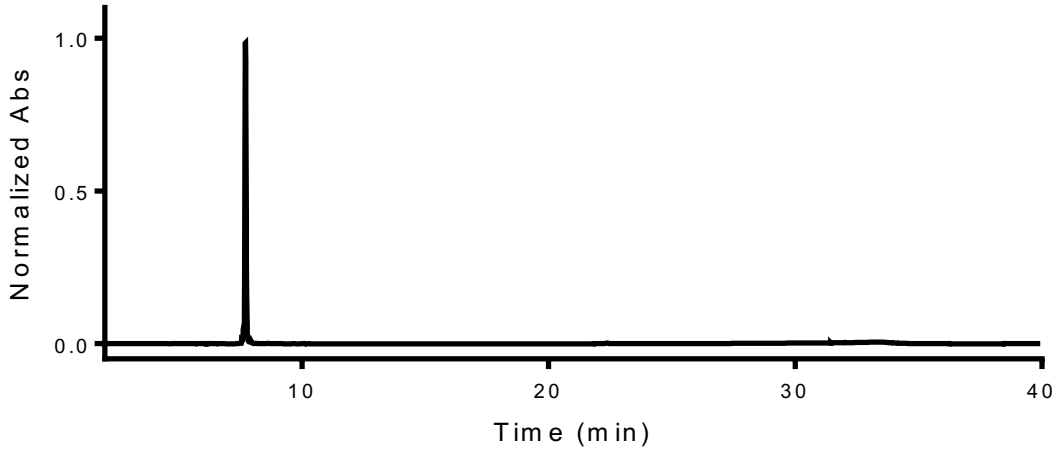

Figure S21. Analytical HPLC chromatogram of **7**.

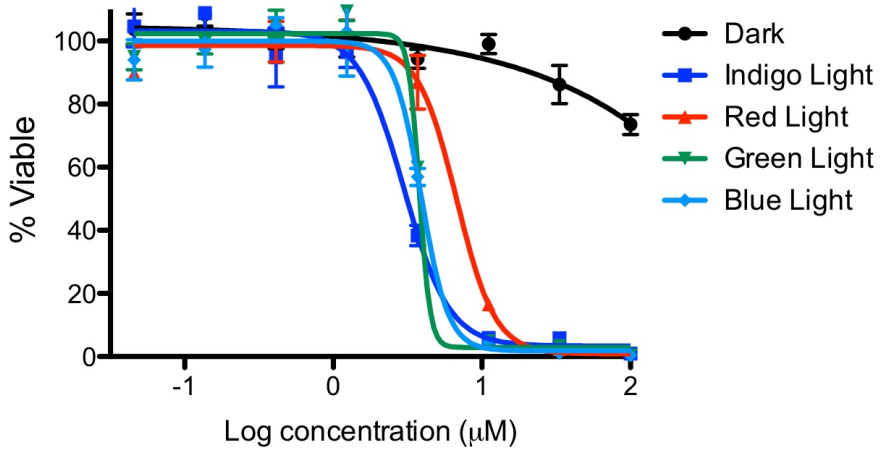

Figure S22. Cell cytotoxicity dose responses for compound **1** with different light sources.

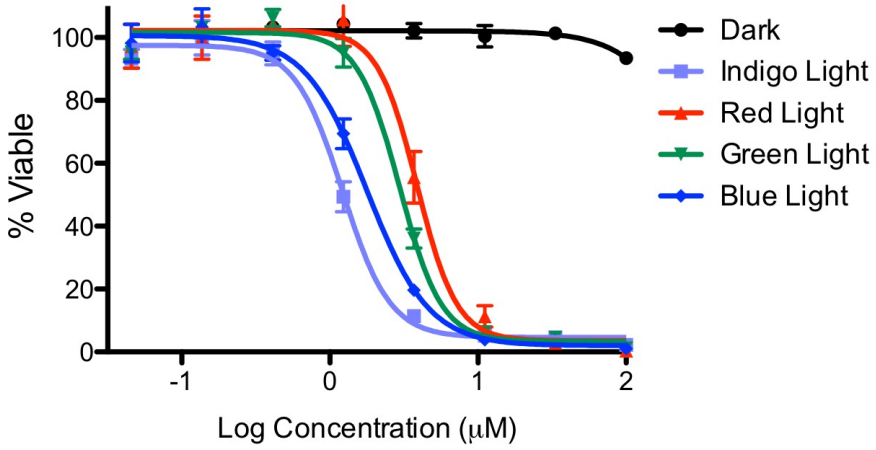

Figure S23. Cell cytotoxicity dose responses for compound **2** with different light sources.

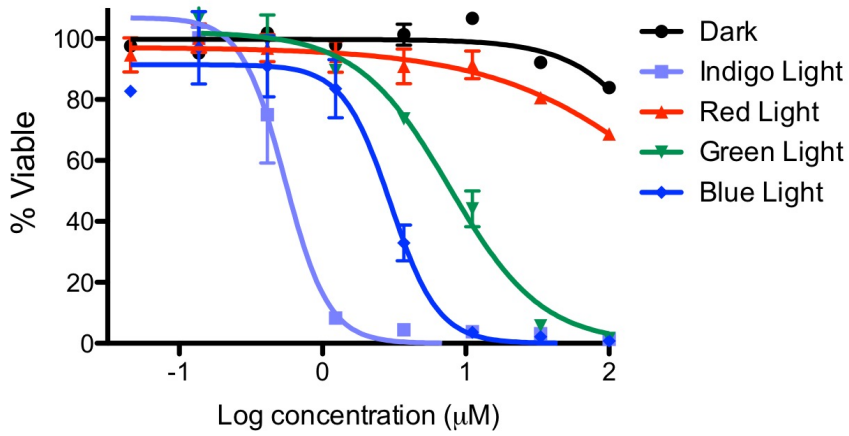

Figure S24. Cell cytotoxicity dose responses for compound **3** with different light sources.

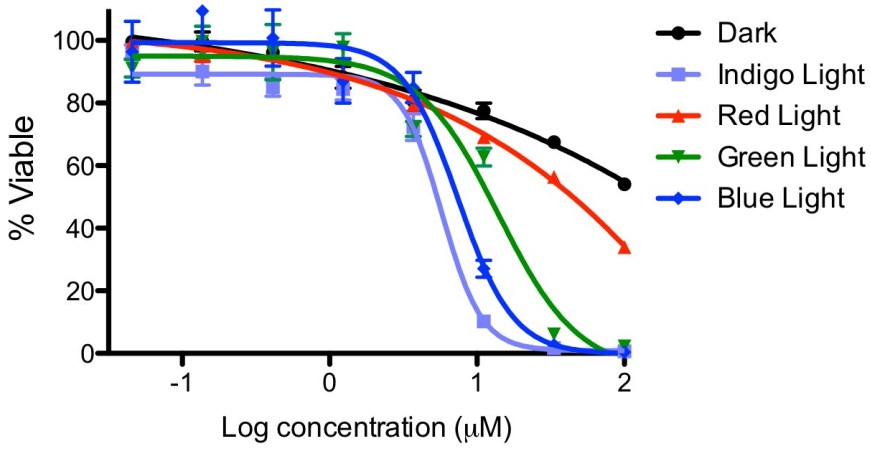

Figure S25. Cell cytotoxicity dose responses for compound **4** with different light sources.

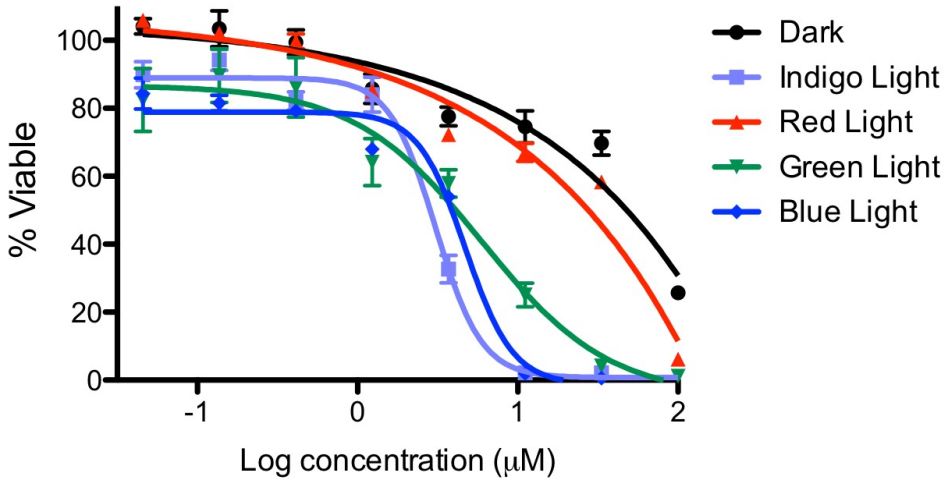

Figure S26. Cell cytotoxicity dose responses for compound **5** with different light sources.

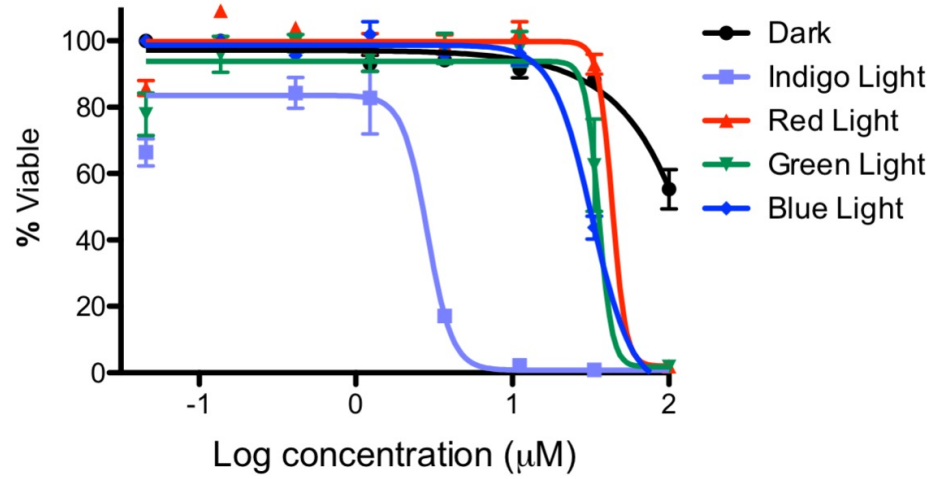

Figure S27. Cell cytotoxicity dose responses for compound **6** with different light sources.

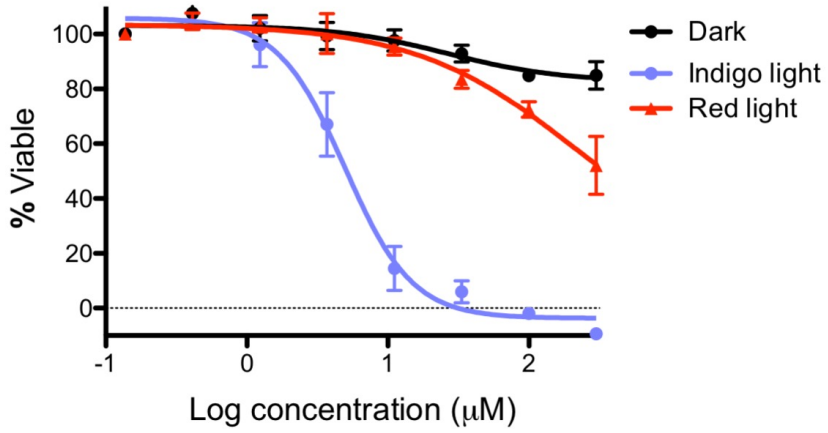

Figure S28. Cell cytotoxicity dose responses for compound **7** with different light sources.

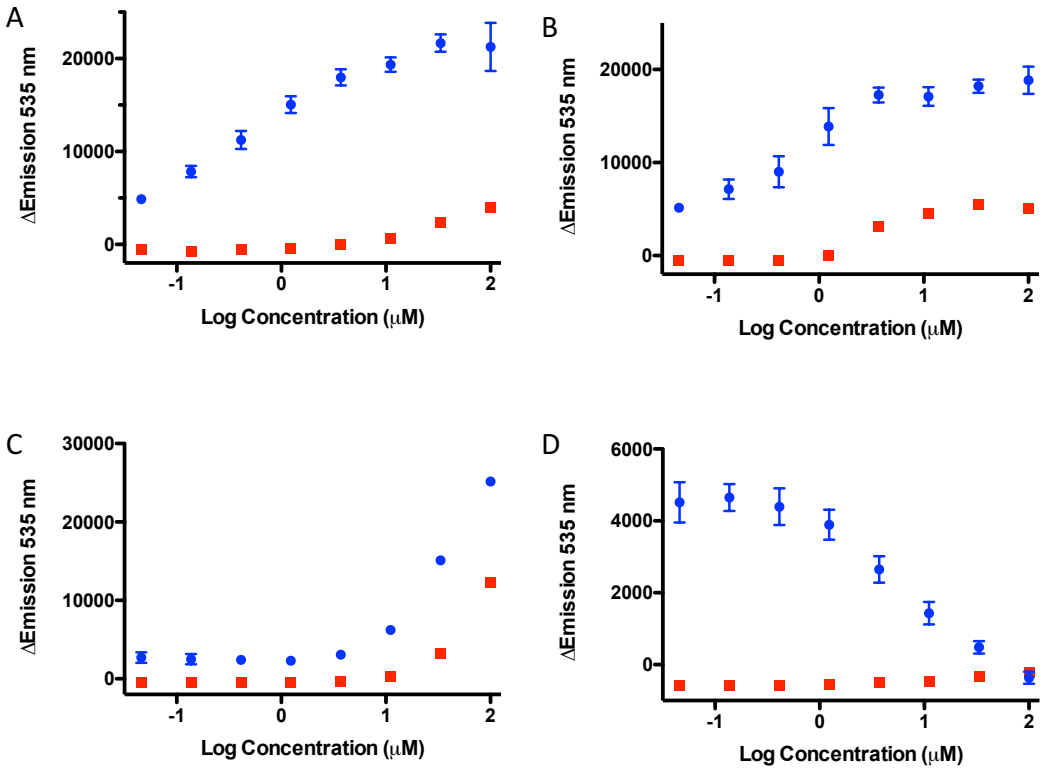

Figure S29. Dose dependent generation of $^1O_2$ detected by SOSG. A) Compound **3**; B) Compound **6**; C) $Ru(dpp)_3$; D) Compound **2**.

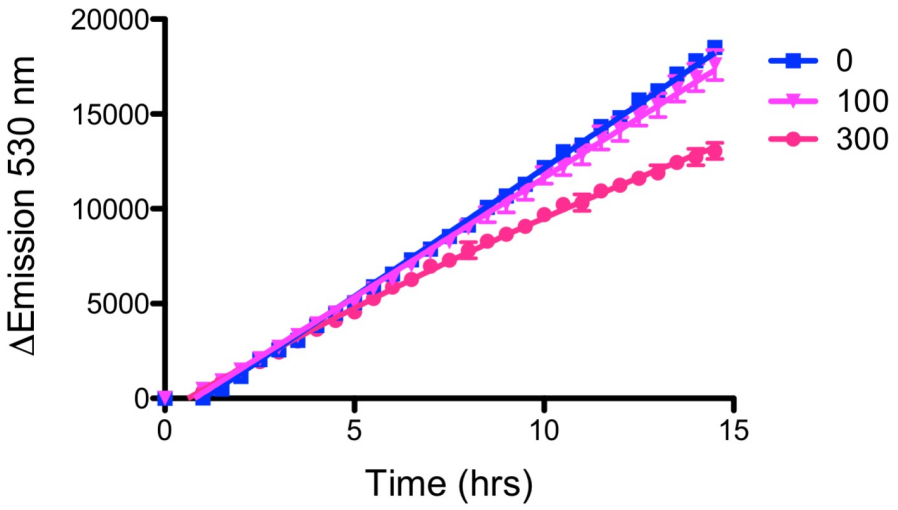

Figure S30. Time dependent inhibition of production of Dendra2 by compound **4** in the dark in HEK293 T-REx cells.

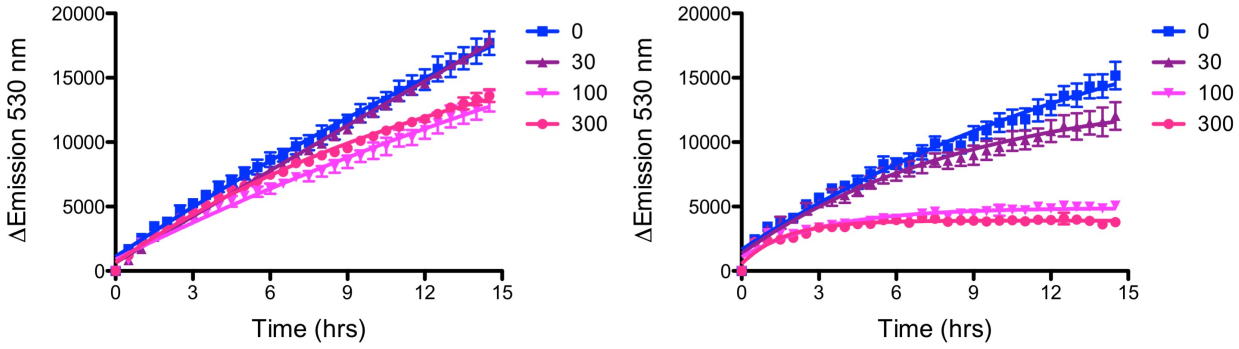

Figure S31. Time dependent inhibition of production of Dendra2 by compound **2** (left) and compound **4** (right) following irradiation in HEK293 T-REx cells.